

Enhancing Layer Attention Efficiency through Pruning Redundant Retrievals

Hanze Li¹, Xiande Huang²

¹Glasgow College, University of Electronic Science and Technology of China

²De AI Lab, De Intelligence Technology Co., Ltd

Abstract

Growing evidence suggests that layer attention mechanisms, which enhance interaction among layers in deep neural networks, have significantly advanced network architectures. However, existing layer attention methods suffer from redundancy, as attention weights learned by adjacent layers often become highly similar. This redundancy causes multiple layers to extract nearly identical features, reducing the model’s representational capacity and increasing training time. To address this issue, we propose a novel approach to quantify redundancy by leveraging the Kullback-Leibler (KL) divergence between adjacent layers. Additionally, we introduce an Enhanced Beta Quantile Mapping (EBQM) method that accurately identifies and skips redundant layers, thereby maintaining model stability. Our proposed Efficient Layer Attention (ELA) architecture, improves both training efficiency and overall performance, achieving a 30% reduction in training time while enhancing performance in tasks such as image classification and object detection.

1 Introduction

Numerous studies have successfully demonstrated that enhancing the representational ability of deep convolutional neural networks (DCNNs) significantly improves their performance across various tasks. For instance, ResNet [He *et al.*, 2016] introduced skip connections to facilitate gradient flow, effectively mitigating the problem of performance degradation in deep networks. DenseNet [Huang *et al.*, 2017] further enhanced model capacity by reusing information from all previous layers. In addition to these innovations, attention mechanisms have further enhanced model performance. Channel attention mechanisms [Hu *et al.*, 2018; Wang *et al.*, 2020b; Qin *et al.*, 2021; Ouyang *et al.*, 2023], refine feature selection by prioritizing significant channels, allowing networks to focus on the most relevant feature maps. Complementing this, spatial attention mechanisms [Woo *et al.*, 2018; Wang *et al.*, 2018; Li *et al.*, 2023a; Wang *et al.*, 2024cl], optimize performance by directing attention to critical spatial

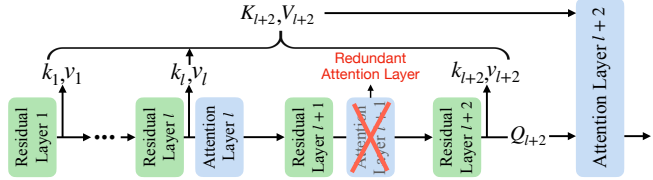
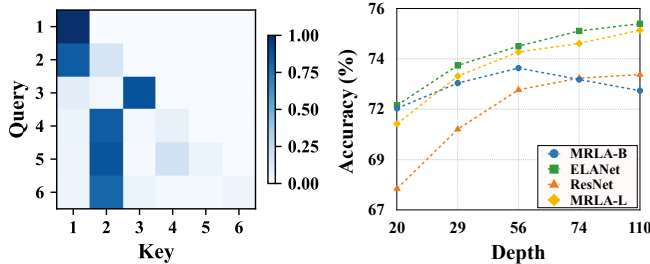


Figure 1: Redundant attention layer in layer attention architecture can be discarded.

regions, improving the network’s ability to capture spatial hierarchies and refine learned representations.

Recently, enhancing interactions between hierarchical layers has emerged as another effective approach to improving model’s representational ability. DIANet [Huang *et al.*, 2020] incorporated a modified LSTM block along the depth of the network to promote the interactions between layers. Similarly, RLANet [Zhao *et al.*, 2021] employs a lightweight recurrent aggregation module to effectively reuse information from previous layers. BViT [Li *et al.*, 2023b] processes the output of each Transformer layer in the ViT [Dosovitskiy, 2020] architecture through attention mechanism, effectively enhancing model’s representational ability and overall performance. To further enhance cross-layer interaction, MRLA [Fang *et al.*, 2023] first introduced layer attention, leveraging a multi-head attention mechanisms across layers to align features from current layer with those of all preceding layers.

However, we have identified a significant drawback in existing layer attention mechanisms: the inherent redundancy within the attention process across layers. As shown in Figure 2a, the attention weights learned by three consecutive layers (the 4th, 5th, and 6th layers) are nearly identical, with the attention focusing on just one layer. This suggests that these layers are extracting almost identical features, which undermines the model’s representational capacity. For instance, in the **MRLA-B** model, as the network depth increases, accuracy drops noticeably, with performance even falling below that of the ResNet baseline, as depicted in Figure 2b. The lightweight layer attention network MRLA-L achieves impressive performance, but continues to struggle with low training efficiency induced by redundancy. Therefore, eliminating redundant attention layers from the layer attention network is essential to maintain both model performance and



(a) Visualization of attention scores with six adjacent layers of MRLA-B, MRLA-L, ELANet, and ResNet in layer attention for ResNet-56 (with ResNet as the backbone) (stage 2). (b) Top1-accuracy comparison and ResNet at varying depths.

Figure 2: Attention map and layer attention model performance on CIFAR-100.

training efficiency, as demonstrated in Figure 1.

To assess redundancy in layer attention networks, we propose using KL divergence to evaluate the similarity of attention weights between adjacent layers. In a layer attention network, the attention weights of each layer can be treated as a probability distribution, and KL divergence measures the difference between these distributions. Specifically, a smaller KL divergence value indicates greater functional similarity between adjacent layers, as shown in Figure 3. Our findings reveal that the distribution of these KL divergences remains stable throughout training. However, some KL divergences may become overly concentrated, making it difficult to accurately identify which layers to prune. To address this, we introduce an innovative algorithm, Enhanced Beta Quantile Mapping (EBQM), which make the KL divergence of distributions suitable for pruning layers. This improves the stability of the model’s performance. Experimental results validate the effectiveness of our method, showing improvements in both speed and accuracy over state-of-the-art techniques across various tasks.

The contributions of this paper are summarized as follows:

- We propose a novel approach that employs KL divergence to assess redundancy in layer attention networks, which quantifies the similarity of attention weights between adjacent layers.
- An innovative algorithm, named EBQM, is introduced to skip redundant attention layers while maintaining model stability.
- Our ELA architecture successfully reduces redundancy in existing layer attention mechanisms, resulting in an approximate 30% increase in training speed and improved performance on various tasks, including image recognition and object detection.

2 Related Work

2.1 Layer Interaction

A growing number of research has focused on layer interaction in deep convolutional neural networks. DIANet [Huang *et al.*, 2020] incorporated a parameter-shared DIA block across all layers to facilitate information flow between layers.

Similarly, RLANet [Zhao *et al.*, 2021] proposed a lightweight recurrent aggregation module that efficiently reuses information from previous layers to improve feature extraction in subsequent layers. [Zhao *et al.*, 2022] integrated information from the preceding layers with the current layer through a dot product operation, significantly improving the model performance. BViT [Li *et al.*, 2023b] applied an attention mechanism to the output of each layer in Vision Transformer (ViT), effectively integrating information throughout the model. ST-UNet [Zhang *et al.*, 2023] proposed a feature enhancement module during the concatenation of the inter-layer feature map in U-Net [Ronneberger *et al.*, 2015], which improves the feature extraction process in each layer. MRLA [Fang *et al.*, 2023] treated the features of each layer as tokens, employing an attention mechanism to promote interaction between hierarchical layers, further reinforcing the connectivity between layers. DLANet [Wang *et al.*, 2024b] employed a modified LSTM module at every layer, ensuring dynamic information update before MRLA attention operation.

2.2 Efficient Attention

Traditional attention mechanisms are often hindered by the $O(n^2)$ complexity, which limits their scalability. Multiple studies, such as [Shen *et al.*, 2021; Ma *et al.*, 2021], addressed this issue by utilizing linear attention structures to reduce the computational complexity. Furthermore, [Li *et al.*, 2022] accelerated attention operations in both NLP and vision tasks by pruning tokens with small attention scores. [Guo *et al.*, 2023] mitigated the issue of Transformers overemphasizing specific tokens by restricting the attention mechanism to the local neighborhood of each token. SKIPAT [Venkataraman *et al.*, 2023] identified the phenomenon of functional similarity in successive layers within vision transformers (ViT) and proposed replacing these redundant transformer layers with a parametric function to enhance efficiency. Similarly, EfficientViT [Liu *et al.*, 2023] employed cascaded group attention to improve attention diversity in ViT, effectively addressing redundancy. Additionally, [Wang *et al.*, 2024a] improved efficiency in ViT by pruning less important or similar tokens from the attention map.

3 Method

We will begin by recalling the existing layer attention architecture and highlighting its redundancy. Next, we will explain how KL divergence can be used to identify redundant attention layers. Finally, we will explain the issue of overly concentrated KL divergences and present our Enhanced Beta Quantile Mapping Algorithm, which resolves this problem and stabilizes model performance.

3.1 Revisiting Layer Attention

Layer attention [Fang *et al.*, 2023] is a novel mechanism that enhances inter-layer dependencies by allowing each layer in a neural network to retrieve query-relevant information from all preceding layers. Given $x^l \in \mathbb{R}^{C \times H \times W}$ as the feature of layer l , the layer attention mechanism is employed as the following formulas:

$$\begin{cases} \mathbf{Q}^l = F_q^l(\mathbf{x}^l), \\ \mathbf{K}^l = \text{Concat} [F_k^1(\mathbf{x}^1), \dots, F_k^l(\mathbf{x}^l)], \\ \mathbf{V}^l = \text{Concat} [F_v^1(\mathbf{x}^1), \dots, F_v^l(\mathbf{x}^l)]. \end{cases} \quad (1)$$

The function F_q^l serves to extract Query from the current layer x^l , while the functions F_k^i and F_v^i are responsible for extracting Key and Value matrix from x^i , where x_i denotes the i -th layer feature. Then the layer attention can be calculated as:

$$\mathbf{O}^l = \mathbf{Q}^l (\mathbf{K}^l)^\top \mathbf{V}^l = \sum_{i=1}^l \mathbf{Q}^l [F_k^i(\mathbf{x}^i)]^\top F_v^i(\mathbf{x}^i) \quad (2)$$

This represents the structure of MRLA-B defined by [Fang *et al.*, 2023]. For clarity, the softmax and the scaling factor in the multihead attention mechanism D_k defined by [Vaswani, 2017] are omitted here. By substituting :

$$\mathbf{Q}^l = \boldsymbol{\lambda}_o^l \odot \mathbf{Q}^{l-1} \quad (3)$$

into Equation(2), a lightweight version, referred to as MRLA-L, can be derived:

$$\mathbf{O}^l = \boldsymbol{\lambda}_o^l \odot \mathbf{O}^{l-1} + \mathbf{Q}^l [F_k^l(\mathbf{x}^l)]^\top F_v^l(\mathbf{x}^l) \quad (4)$$

In this case, $\boldsymbol{\lambda}_o^l$ is defined as a learnable vector to dynamically adjust the contribution of prior layers during the attention process.

3.2 Motivation

MRLA leverages a multihead attention mechanism to strengthen inter-layer interactions. However, a key limitation of MRLA is the redundancy observed within the network, where the attention weights learned by certain adjacent attention layers are very similar. This similarity indicates that these layers extract nearly identical features. To further investigate this phenomenon, we utilized the Score-CAM [Wang *et al.*, 2020a] method to visualize the outputs of sequential MRLA layers, as shown in Figure 3. The figure presents the feature map visualizations of successive MRLA layers in ResNet-101, using images from the ImageNet-1K dataset. The results demonstrate that when the KL divergence between the attention weights of two MRLA layers is small, their feature maps are remarkably similar, highlighting their functional redundancy. Moreover, the number of such redundant layers increases with network depth, leading to a gradual decline in the model’s representation capability and an unnecessary increase in training time.

The presence of redundant attention layers undermines the capability of the original backbone network, as numerous layers end up performing identical tasks. Skipping these redundant attention layers while retaining the original backbone layers allows the network to both leverage the layer attention mechanism to retrieve information from previous layers and ensure feature diversity across layers. This approach enhances the model’s capacity and reduces training time without introducing additional parameters. Therefore, this paper aims to develop an innovative method to identify and precisely skip these redundant layers.

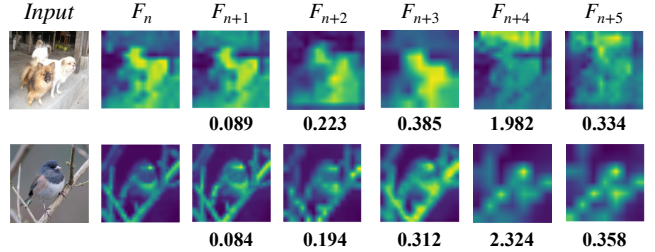


Figure 3: Visualization of feature maps from consecutive six attention Layers on ResNet-101. The values below each feature map represent the KL divergence of the attention weights between the F_t and F_{t-1} layers.

3.3 Layer Pruning Based on KL Divergence

KL Divergence In our approach, we employ the KL divergence to measure the difference between probability distributions derived from the attention weights of adjacent layers in a neural network. The KL divergence between two discrete probability distributions $P = \{p_1, p_2, \dots, p_n\}$ and $P' = \{p'_1, p'_2, \dots, p'_n\}$ is defined as:

$$D_{\text{KL}}(P \parallel P') = \sum_i p_i \log \left(\frac{p_i}{p'_i} \right) \quad (5)$$

Here, p_i and p'_i represent the probabilities from distributions P and P' , respectively. The KL divergence quantifies the difference between these two distributions, where a smaller KL divergence indicates that the two distributions are more similar, while a larger value reflects greater dissimilarity.

KL Divergence in Layer Attention Let the output of the l -th layer be denoted as $\mathbf{x}^l \in \mathbb{R}^{C \times H \times W}$, where C , H , and W represent the number of channels, height, and width, respectively. The output \mathbf{x}^l can be expressed as a linear combination of features:

$$\mathbf{x}^l = p_1 v_1 + p_2 v_2 + \dots + p_l v_l \quad (6)$$

where $v_i = F_v^i(\mathbf{x}^i)$ is the i -th value in V^l , and $P = \{p_1, p_2, \dots, p_l\}$ represents the distribution of attention weights.

Similarly, the output of the $l+1$ -th layer, $\mathbf{x}^{l+1} \in \mathbb{R}^{C \times H \times W}$, is given by:

$$\mathbf{x}^{l+1} = p'_1 v_1 + p'_2 v_2 + \dots + p'_{l+1} v_{l+1} \quad (7)$$

where $\{p'_1, p'_2, \dots, p'_{l+1}\}$ is another probability distribution P' derived from the attention mechanism at the $l+1$ -th layer. Notably, the distribution P' has one additional value p'_{l+1} compared to P .

To ensure the two distributions are comparable, we append an infinitesimally small value ϵ (where $\epsilon \rightarrow 0$) to the distribution P so that it matches the dimensionality of P' , i.e., $P = \{p_1, p_2, \dots, p_l, \epsilon\}$

We then compute the KL divergence between these distributions using the standard formula:

$$D_{\text{KL}}(P \parallel P') = \sum_{i=1}^l p_i \log \left(\frac{p_i}{p'_i} \right) + \epsilon \log \left(\frac{\epsilon}{p'_{l+1}} \right) \quad (8)$$

In a layer attention network, the feature maps v_1, v_2, \dots, v_{l+1} remain consistent between layers l and $l+1$, which means that the difference between the outputs of the two layers is entirely determined by the difference in their attention weight distributions P and P' . The KL divergence between P and P' thus directly reflects the similarity between the outputs x^l and x^{l+1} , as demonstrated in Figure 3.

Attention-Layer Pruning Algorithm A training process is divided into several stages, and in each stage, we begin by calculating the KL divergences between the attention weights of adjacent MRLA layers. Here we do not explicitly define the number of layers to skip. This is because, at each training stage (except the initial one), the KL divergence distribution is influenced by the results of the previous stage, which affects the number of layers to be discarded. If the same number of layers is removed from each stage, some critical attention layers in certain stages may be discarded, which can degrade the model's performance, as demonstrated in the results of Table 4. However, within each individual training stage, the distribution of KL divergence remains relatively stable.

The proposed algorithm for layer pruning, as detailed in Algorithm 1, uses a threshold μ to determine which layers to discard. Initially, we focus on KL divergence values below the computed γ -quantile and normalize these values to the range $x \in [0, 1]$ for ease of threshold configuration. However, in certain cases, the normalized KL divergence values tend to cluster within a narrow range. If a single threshold μ is applied, even small fluctuations in KL divergence values across different training runs or stages can lead to significant variations in the number of skipped MRLA layers. For instance, if the threshold μ is set to 0.3, six layers with KL divergence values ranging from 0.31 to 0.33 in one training run may fall within the range of 0.27 to 0.29 in another. This discrepancy results in a six-layer difference in the layers skipped between the two runs. Although limiting the normalization process to KL divergence values below the γ -quantile alleviates the issue to some extent, it still has a substantial impact on model performance and robustness, as shown in Table 4.

To address this issue, we propose preprocessing the distribution of normalized KL divergence values prior to thresholding. Inspired by the Quantile Mapping Algorithm, a technique widely applied in meteorology and hydrology to align disorganized data with a target distribution, we propose an innovative **Enhanced Beta Quantile Mapping (EBQM)** Algorithm to reshape the distribution of values. Here, we reshape the data using the cumulative distribution function (CDF) of the Beta distribution.

The CDF of a Beta distribution can be illustrated in mathematical terms:

$$\text{CDF}_{\text{Beta}}(x) = \begin{cases} 0 & \text{if } x < 0, \\ F_{\text{Beta}}(x; \alpha, \beta), & \text{if } 0 \leq x \leq 1, \\ 1 & \text{if } x > 1. \end{cases}$$

$F_{\text{Beta}}(x; \alpha, \beta)$ on the interval $[0, 1]$, is given by:

$$F_{\text{Beta}}(x; \alpha, \beta) = \int_0^x \frac{t^{\alpha-1}(1-t)^{\beta-1}}{B(\alpha, \beta)} dt \quad (9)$$

Algorithm 1 Enhanced Beta Quantile Mapping (EBQM)

Input: KL divergences from layer 1 to layer l : $[x_1, x_2, \dots, x_l]$
Parameter: Quantile γ , Beta distribution parameters α, β , threshold ϵ , number of epochs E
Output: Updated KL divergences $[x_1, \dots, x_l]$ with skipped layers

- 1: **for** epoch $e = 1$ to E **do**
- 2: Sort KL divergences in ascending order:

$$[x_1, x_2, \dots, x_l] \rightarrow [x_{(1)}, x_{(2)}, \dots, x_{(l)}]$$

$$x_{(1)} \leq x_{(2)} \leq \dots \leq x_{(l)}$$
- 3: Extract γ -quantile:

$$S_\gamma = \{x_i \mid x_i \leq Q_\gamma\}, \quad Q_\gamma = \gamma\text{-quantile of } [x_1, \dots, x_l]$$
- 4: **for** each $x_j \in S_\gamma$ **do**
- 5: Normalize x_j :

$$x'_j = \frac{x_j - \min(S_\gamma)}{\max(S_\gamma) - \min(S_\gamma)}$$
- 6: Apply Beta CDF: $y_j = F_{\text{Beta}}(x'_j; \alpha, \beta)$
- 7: **if** $y_j < \mu$ **then**
- 8: Skip layer: Set $x_j = -1$
- 9: **end if**
- 10: **end for**
- 11: **end for**
- 12: **return** Updated KL divergences $[x_1, \dots, x_l]$

where $\alpha > 0$ and $\beta > 0$ are shape parameters, and $B(\alpha, \beta)$ is the Beta function, expressed as:

$$B(\alpha, \beta) = \int_0^1 t^{\alpha-1}(1-t)^{\beta-1} dt \quad (10)$$

Unlike other distribution functions, such as the Gamma distribution, the CDF of the Beta distribution is uniquely defined within the $[0, 1]$ interval for both its input and output. This property aligns perfectly with the normalized KL divergence values we aim to reshape, as they also fall within the $[0, 1]$ range. Consequently, the normalized KL divergence values can be directly utilized as inputs to the Beta distribution's CDF for efficient and precise distribution reshaping. By applying this Beta-distribution-based transformation before thresholding, and adjusting the parameters α and β , we can effectively disperse clustered values under almost all conditions.

4 Experiments

4.1 Image Classification

We carried out experiments on the CIFAR-10, CIFAR-100, and ImageNet-1K [Deng *et al.*, 2009] datasets, utilizing ResNet [He *et al.*, 2016] as the backbone compared with various baselines, such as channel attention methods, spatial attention models, and other layer interaction methods. For the CIFAR-10 and CIFAR-100 datasets, we applied the data augmentation techniques described in [Huang *et al.*, 2016]. For the ImageNet-1K dataset, the augmentation techniques

and hyperparameter configurations followed those specified by [He *et al.*, 2016; He *et al.*, 2019].

Experimental Settings When training on CIFAR-10 and CIFAR-100 datasets, α and β were set to 5 and 1, respectively, and μ set to 0.3. We trained for a total of 180 epochs, averaging the KL divergence values from the first to the third epoch to determine the final data to discard. This process was repeated during the 45th to 48th epochs and again during the 91st to 93rd epochs. Furthermore, the model was trained on ImageNet-1K for 100 epochs. The KL divergence values were averaged over the first to third epochs and the 51st to 53rd epochs to guide layer pruning. Consistent with the CIFAR settings, α and β were set to 2 and 5, respectively, with the threshold μ adjusted to 0.25.

Results on CIFAR-10 and CIFAR-100 ELANet, which integrates the proposed method of pruning attention operations from certain layers, demonstrates a clear advantage over baseline models on both CIFAR-10 and CIFAR-100. As shown in Table 1, ELA achieves 92.45% and 71.67% top-1 accuracy on the ResNet-20 backbone, surpassing ResNet-20 by 1.10% and 3.72% on CIFAR-10 and CIFAR-100, respectively. ELA also outperforms several channel and spatial attention models, such as SE [Hu *et al.*, 2018], BAM [Park, 2018], and CBAM [Woo *et al.*, 2018]. In the ResNet-56 backbone, ELA surpasses SE, BAM, and CBAM by 0.59%, 0.71%, and 0.39% on CIFAR-10, and by 0.53%, 0.67%, and 0.60% on CIFAR-100, respectively, with lower parameters introduced. Furthermore, in the ResNet-110, our model exceeds a number of layer interaction models, surpassing DIA[Huang *et al.*, 2020] and MRLA-L [Fang *et al.*, 2023] by 0.39% and 0.38% on CIFAR-10, and by 0.21% and 0.33% on CIFAR-100, respectively. These results highlight ELA’s superior classification performance while maintaining efficient parameter usage across various network depths.

ELA significantly reduces training time. As shown in Figure 4, the training time for the three networks on CIFAR-10 and CIFAR-100 are nearly identical for one epoch, with MRLA-B exhibiting the longest training time. Compared to MRLA-B, MRLA-L reduces training time by approximately 10%-15%, while the proposed ELA achieves an even greater reduction, decreasing training time by around 30%-35% relative to the original MRLA-B. Moreover, the reduction in training time becomes more significant as the number of network layers increases.

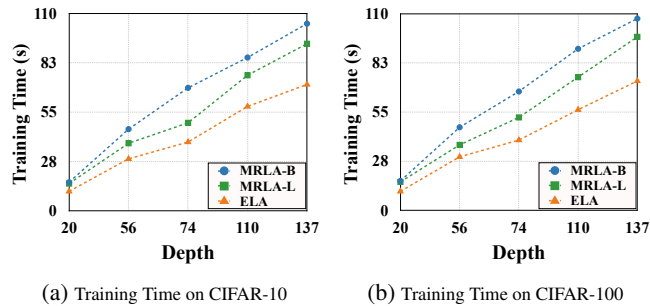


Figure 4: Comparison of per epoch training time (in seconds) for different models with varying depths under identical training conditions.

Models	CIFAR-10		CIFAR-100	
	Params	Top-1	Params	Top-1
ResNet-20	0.22M	91.35	0.24M	67.95
SE	0.24M	91.22	0.27M	68.61
ECA	0.22M	91.45	0.24M	67.35
DIA	0.44M	92.02	0.46M	68.83
CBAM	0.24M	91.97	0.27M	67.71
BAM	0.27M	91.87	0.29M	67.91
MRLA-L	0.23M	92.21	0.25M	70.84
ELA	0.23M	92.45	0.25M	71.67
ResNet-56	0.59M	93.01	0.61M	72.36
SE	0.66M	93.56	0.68M	73.78
ECA	0.59M	94.11	0.61M	73.38
DIA	0.81M	93.56	0.83M	74.01
CBAM	0.66M	93.76	0.68M	73.71
BAM	0.73M	93.44	0.75M	73.64
MRLA-L	0.62M	93.88	0.64M	74.13
ELA	0.62M	94.15	0.64M	74.31
ResNet-110	1.15M	92.94	1.17M	73.04
SE	1.28M	94.30	1.30M	75.18
ECA	1.15M	94.27	1.17M	75.08
DIA	1.37M	94.13	1.39M	75.14
CBAM	1.28M	93.79	1.30M	74.87
BAM	1.42M	93.84	1.45M	74.99
MRLA-L	1.21M	94.14	1.23M	75.02
ELA	1.21M	94.52	1.23M	75.35

Table 1: Top-1 accuracy (%) of different models with ResNet backbone on CIFAR-10 and CIFAR-100.

Results on ImageNet-1K We compare ELA with a range of state-of-the-art models, using ResNet as backbone. As shown in Table 2, ELA achieves 77.9% Top-1 accuracy on the ResNet-50, an improvement of 1.8% over its backbone. Compared to attention-based models like SE and CBAM, ELA offers 1.2% and 0.6% higher Top-1 accuracy, respectively, while using a smaller number of parameters. Moreover, ELA outperforms A^2 [Chen *et al.*, 2018] by 0.9%, AA [Bello *et al.*, 2019] by 0.2%, and GC [Cao *et al.*, 2019] by 0.2%. Furthermore, ELA performs better than MRLA-L, which achieves 77.7%, by 0.2% in the accuracy of Top-1. For the deeper ResNet-101 backbone, ELA again delivers the best performance, achieving 78.8% in Top-1 accuracy, surpassing ResNet-101 by 1.4%. It also outperforms SE, CBAM, and AA by 0.2%, 0.3%, and 0.1%, respectively. Notably, ELA achieves 0.1% higher Top-1 accuracy than MRLA-L, which reaches 78.7%. When compared to lightweight models such as ECA, ELA provides an additional 0.4% improvement in Top-1 accuracy for ResNet-50 and 0.1% for ResNet-101, despite a slight increase in parameters. The results demonstrate that ELA significantly outperforms other models in terms of Top-1 and Top-5 accuracy, while maintaining competitive computational efficiency.

A significant reduction in training time for ELA on the ImageNet-1K dataset is presented in Table 3. ELA reduces the training time per epoch by 29.7% compared to MRLA-

B for ResNet-50 and by 32.6% for ResNet-101, outperforming MRLA-L, which achieves reductions of only 13.5% and 16.3% for ResNet-50 and ResNet-101, respectively. Furthermore, as the number of network layers increases, the proportion of training time reduction compared with MRLA-B becomes more pronounced.

Models	Params	FLOPs	Top-1	Top-5
ResNet-50	25.6M	4.1B	76.1	92.9
SE	28.1M	4.1B	76.7	93.4
CBAM	28.1M	4.2B	77.3	93.7
A^2	34.6M	7.0B	77.0	93.5
AA	27.1M	4.5B	77.7	93.8
GC	29.4M	4.2B	77.7	93.7
ECA	25.6M	4.1B	77.5	93.7
RLA	25.9M	4.5B	77.2	93.4
MRLA-L	25.7M	4.2B	77.7	93.8
MRLA-B	25.7M	4.6B	77.7	93.9
ELA	25.7M	4.4B	77.9	94.1
ResNet-101	44.5M	7.8B	77.4	93.5
SE	49.3M	7.8B	77.6	93.9
CBAM	49.3M	7.9B	78.5	94.3
AA	47.6M	8.6B	78.7	94.4
ECA	44.5M	7.8B	78.7	94.3
RLA	45.0M	8.4B	78.5	94.2
MRLA-L	44.9M	7.9B	78.7	94.4
ELA	44.9M	8.1B	78.8	94.6

Table 2: Top-1 and Top-5 accuracy (%) of different models with ResNet backbone on ImageNet-1K.

Depth	Models	Training Time (h)
50	MRLA-B	3.7
	MRLA-L	3.2
	ELA	2.6
101	MRLA-B	8.6
	MRLA-L	7.2
	ELA	5.8

Table 3: Comparison of per epoch training time (in hours) for different models with varying depths under identical training conditions on ImageNet-1K.

4.2 Object Detection

Experimental Settings In the object detection task, our approach was evaluated on the COCO2017 dataset using Faster R-CNN and Mask R-CNN as detectors. All models were implemented using the open-source MMDetection toolkit [Chen *et al.*, 2019] to ensure consistency and reproducibility, with all configurations following the default MMDetection settings. Each detector underwent 12 training epochs, with KL divergence measured at the 1st and 7th epochs to analyze layer significance at early and later training stages. The hyperparameters α and β were set to 2 and 5, respectively, while μ was fixed at 0.2.

Results on COCO2017 Our proposed ELA method achieves significant improvements in object detection performance compared to several state-of-the-art methods across various backbone networks and detectors. As highlighted in Table 5, when Faster R-CNN is used with ResNet-50, ELA outperforms SE, ECA, and RLA [Zhao *et al.*, 2021] by achieving 40.5% in AP, a gain of 2.8% over SE, 2.5% over ECA and 1.7% over RLA. It also shows improvements in AP₅₀ and AP₇₅, highlighting its superiority in detecting objects across different scales. With ResNet-101, ELA continues to show competitive performance, surpassing not only MRLA-L, but also SE, ECA, and other models, with a 0.1% improvement in AP and a notable increase in AP₅₀ and AP₇₅. Similarly, when Mask R-CNN is used as the detector, ELA maintains its edge, achieving a 0.2% increase in AP compared to MRLA-L on ResNet-50, and showing substantial improvements over methods like NL [Wang *et al.*, 2018] and GC [Cao *et al.*, 2019]. These results confirm that ELA consistently enhances object detection accuracy, offering a balanced trade-off between performance and computational efficiency.

5 Ablation Studies

5.1 Evaluation of Different Layer Pruning Methods

To evaluate the effectiveness of EBQM, we conducted comparative experiments with two alternative strategies. First, a fixed layer pruning strategy was employed, where the number of pruned layers was determined by a hyperparameter. The pruned layer count was aligned as closely as possible with the number determined by Algorithm 1. Second, a threshold-based pruning strategy was implemented, using a fixed hyperparameter to define a KL divergence threshold: layers with values below the threshold were discarded, while those above were retained. The ablation experiments were conducted on CIFAR-100 using ResNet [He *et al.*, 2016] architectures of varying depths as baselines. Each experiment was repeated five times, and results were reported as *Accuracy \pm Standard Deviation* to evaluate the model’s robustness and performance.

As shown in Table 4, it is evident that as the network depth increases, the instability of the Threshold-Based method also increases. The standard deviation rises from 0.44% in ResNet-56 to 0.79% in ResNet-110. A similar trend is observed with the Fixed Layer Pruning method. In contrast, the Top-1 accuracy achieved by our EBQM is consistently

Depth	Methods	Top-1
56	Threshold-Based	73.89 \pm 0.44
	Fixed Layer Pruning	73.79 \pm 0.30
	EBQM	74.31\pm0.24
110	Threshold-Based	74.83 \pm 0.79
	Fixed Layer Pruning	74.92 \pm 0.41
	EBQM	75.35\pm0.22

Table 4: Top-1 accuracy (%) of different methods for redundant layer pruning with ResNet backbone on CIFAR-100.

Detectors	Methods	Params	AP	AP ₅₀	AP ₇₅	AP _S	AP _M	AP _L
Faster R-CNN	ResNet-50	41.5M	36.4	58.2	39.2	21.8	40.0	46.2
	SE	44.0M	37.7	60.1	40.9	22.9	41.9	48.2
	ECA	41.5M	38.0	60.6	40.9	23.4	42.1	48.0
	RLA	41.8M	38.8	59.6	42.0	22.5	42.9	49.5
	MRLA-L	41.7M	40.4	61.5	44.0	24.2	44.1	52.7
	ELA	41.7M	40.5	61.6	44.2	24.3	44.3	52.9
	ResNet-101	60.5M	38.7	60.6	41.9	22.7	43.2	50.4
	SE	65.2M	39.6	62.0	43.1	23.7	44.0	51.4
	ECA	60.5M	40.3	62.9	44.0	24.5	44.7	51.3
	RLA	60.9M	41.2	61.8	44.9	23.7	45.7	53.8
	MRLA-L	60.9M	42.0	63.1	45.7	25.0	45.8	55.4
	ELA	60.9M	42.1	63.3	45.8	25.2	45.9	55.5
Mask R-CNN	ResNet-50	44.2M	37.2	58.9	40.3	34.1	55.5	36.2
	SE	46.7M	38.7	60.9	42.1	35.4	57.4	37.8
	ECA	44.2M	39.0	61.3	42.1	35.6	58.1	37.7
	NL	46.5M	38.0	59.8	41.0	34.7	56.7	36.6
	GC	46.9M	39.4	61.6	42.4	35.7	58.4	37.6
	RLA	44.4M	39.5	60.1	43.4	35.6	56.9	38.0
	MRLA-L	44.3M	41.2	62.3	45.1	37.1	59.1	39.6
	ELA	44.3M	41.4	62.4	45.2	37.3	59.2	39.8
	ResNet-101	63.2M	39.4	60.9	43.3	35.9	57.7	38.4
	SE	67.9M	40.7	62.5	44.3	36.8	59.3	39.2
	ECA	63.2M	41.3	63.1	44.8	37.4	59.9	39.8
	NL	65.5M	40.8	63.1	44.5	37.1	59.9	39.2
	GC	82.2M	41.7	63.7	45.5	37.6	60.5	39.8
	RLA	63.6M	41.8	62.3	46.2	37.3	59.2	40.1
	MRLA-L	63.5M	42.8	63.6	46.5	38.4	60.6	41.0
	ELA	63.5M	42.9	63.7	46.7	38.6	60.7	41.2

Table 5: Object detection results on the COCO2017 dataset using various methods with Mask R-CNN and Faster R-CNN detectors

higher than that of the other two methods, reaching 74.31% and 75.35% for ResNet-56 and ResNet-110, respectively.

5.2 Evaluation of Different Distributions and Activation Functions in EBQM

We also investigated whether the selection of the Beta distribution in EBQM outperforms other distributions or activation functions. To this end, we replaced the Beta distribution with commonly used alternatives, such as the Gamma and Normal distributions, as well as activation functions like Softmax and Sigmoid.

Depth	Distributions	Top-1
56	Normal	73.92 \pm 0.39
	Gamma	74.11 \pm 0.33
	Beta	74.31\pm0.24
110	Normal	74.89 \pm 0.44
	Gamma	75.12 \pm 0.34
	Beta	75.35\pm0.22

Table 6: Top-1 accuracy (%) of different kinds of distributions and activation functions in EBQM with ResNet backbone on CIFAR-100.

The Beta distribution outperforms both the Normal and Gamma distributions, as well as the Softmax and Sigmoid functions, in terms of Top-1 accuracy, achieving 74.31% and 75.35% for ResNet-56 and ResNet-110, respectively, as shown in Table 6. Furthermore, the Beta distribution exhibits superior stability, with the lowest standard deviations of 0.24% and 0.22%, indicating more consistent performance compared to the other distributions.

6 Conclusion

In this paper, we uncover the inherent redundancy in existing layer attention mechanisms, characterized by the high similarity of attention weights learned by adjacent layers. We further analyze the two key issues caused by this redundancy: degraded model performance and extended training time. To address these challenges, we propose a novel approach that first evaluates the importance of each attention layer using KL divergence and then employs an Enhanced Beta Quantile Mapping Algorithm to prune redundant layers. Experimental results on image classification and object detection tasks demonstrate that our method effectively eliminates redundant information, resulting in a network that outperforms the original layer attention model.

References

[Bello *et al.*, 2019] Irwan Bello, Barret Zoph, Ashish Vaswani, Jonathon Shlens, and Quoc V Le. Attention augmented convolutional networks. In *Proceedings of the IEEE/CVF international conference on computer vision*, pages 3286–3295, 2019.

[Cao *et al.*, 2019] Yue Cao, Jiarui Xu, Stephen Lin, Fangyun Wei, and Han Hu. Gcnets: Non-local networks meet squeeze-excitation networks and beyond. In *Proceedings of the IEEE/CVF international conference on computer vision workshops*, pages 0–0, 2019.

[Chen *et al.*, 2018] Yunpeng Chen, Yannis Kalantidis, Jian-shu Li, Shuicheng Yan, and Jiashi Feng. A²-nets: Double attention networks. *Advances in neural information processing systems*, 31, 2018.

[Chen *et al.*, 2019] Kai Chen, Jiaqi Wang, Jiangmiao Pang, Yuhang Cao, Yu Xiong, Xiaoxiao Li, Shuyang Sun, Wansen Feng, Ziwei Liu, Jiarui Xu, et al. Mmdetection: Open mmlab detection toolbox and benchmark. *arXiv preprint arXiv:1906.07155*, 2019.

[Deng *et al.*, 2009] Jia Deng, Wei Dong, Richard Socher, Li-Jia Li, Kai Li, and Li Fei-Fei. Imagenet: A large-scale hierarchical image database. In *2009 IEEE conference on computer vision and pattern recognition*, pages 248–255. Ieee, 2009.

[Dosovitskiy, 2020] Alexey Dosovitskiy. An image is worth 16x16 words: Transformers for image recognition at scale. *arXiv preprint arXiv:2010.11929*, 2020.

[Fang *et al.*, 2023] Yanwen Fang, Yuxi Cai, Jintai Chen, Jingyu Zhao, Guangjian Tian, and Guodong Li. Cross-layer retrospective retrieving via layer attention. *arXiv preprint arXiv:2302.03985*, 2023.

[Guo *et al.*, 2023] Yong Guo, David Stutz, and Bernt Schiele. Robustifying token attention for vision transformers. In *Proceedings of the IEEE/CVF International Conference on Computer Vision*, pages 17557–17568, 2023.

[He *et al.*, 2016] Kaiming He, Xiangyu Zhang, Shaoqing Ren, and Jian Sun. Deep residual learning for image recognition. In *Proceedings of the IEEE conference on computer vision and pattern recognition*, pages 770–778, 2016.

[He *et al.*, 2019] Tong He, Zhi Zhang, Hang Zhang, Zhongyue Zhang, Junyuan Xie, and Mu Li. Bag of tricks for image classification with convolutional neural networks. In *Proceedings of the IEEE/CVF conference on computer vision and pattern recognition*, pages 558–567, 2019.

[Heo *et al.*, 2019] Jun-Haeng Heo, Hyunjun Ahn, Ju-Young Shin, Thomas Rodding Kjeldsen, and Changsam Jeong. Probability distributions for a quantile mapping technique for a bias correction of precipitation data: A case study to precipitation data under climate change. *Water*, 11(7):1475, 2019.

[Hu *et al.*, 2018] Jie Hu, Li Shen, and Gang Sun. Squeeze-and-excitation networks. In *Proceedings of the IEEE conference on computer vision and pattern recognition*, pages 7132–7141, 2018.

[Huang *et al.*, 2016] Gao Huang, Yu Sun, Zhuang Liu, Daniel Sedra, and Kilian Q Weinberger. Deep networks with stochastic depth. In *Computer Vision–ECCV 2016: 14th European Conference, Amsterdam, The Netherlands, October 11–14, 2016, Proceedings, Part IV 14*, pages 646–661. Springer, 2016.

[Huang *et al.*, 2017] Gao Huang, Zhuang Liu, Laurens Van Der Maaten, and Kilian Q Weinberger. Densely connected convolutional networks. In *Proceedings of the IEEE conference on computer vision and pattern recognition*, pages 4700–4708, 2017.

[Huang *et al.*, 2020] Zhongzhan Huang, Senwei Liang, Mingfu Liang, and Haizhao Yang. Dianet: Dense-and-implicit attention network. In *Proceedings of the AAAI Conference on Artificial Intelligence*, volume 34, pages 4206–4214, 2020.

[Li *et al.*, 2022] Zheng Li, Soroush Ghodrati, Amir Yazdanbakhsh, Hadi Esmaeilzadeh, and Mingu Kang. Accelerating attention through gradient-based learned runtime pruning. In *Proceedings of the 49th Annual International Symposium on Computer Architecture*, pages 902–915, 2022.

[Li *et al.*, 2023a] Jiafeng Li, Ying Wen, and Lianghua He. Scconv: Spatial and channel reconstruction convolution for feature redundancy. In *Proceedings of the IEEE/CVF Conference on Computer Vision and Pattern Recognition*, pages 6153–6162, 2023.

[Li *et al.*, 2023b] Nannan Li, Yaran Chen, Weifan Li, Zixiang Ding, Dongbin Zhao, and Shuai Nie. Bvit: Broad attention-based vision transformer. *IEEE Transactions on Neural Networks and Learning Systems*, 2023.

[Liu *et al.*, 2023] Xinyu Liu, Houwen Peng, Ningxin Zheng, Yuqing Yang, Han Hu, and Yixuan Yuan. Efficientvit: Memory efficient vision transformer with cascaded group attention. In *Proceedings of the IEEE/CVF Conference on Computer Vision and Pattern Recognition*, pages 14420–14430, 2023.

[Ma *et al.*, 2021] Xuezhe Ma, Xiang Kong, Sinong Wang, Chunting Zhou, Jonathan May, Hao Ma, and Luke Zettlemoyer. Luna: Linear unified nested attention. *Advances in Neural Information Processing Systems*, 34:2441–2453, 2021.

[Ouyang *et al.*, 2023] Daliang Ouyang, Su He, Guozhong Zhang, Mingzhu Luo, Huaiyong Guo, Jian Zhan, and Zhi-jie Huang. Efficient multi-scale attention module with cross-spatial learning. In *ICASSP 2023-2023 IEEE International Conference on Acoustics, Speech and Signal Processing (ICASSP)*, pages 1–5. IEEE, 2023.

[Park, 2018] J Park. Bam: Bottleneck attention module. *arXiv preprint arXiv:1807.06514*, 2018.

[Piani *et al.*, 2010] Claudio Piani, JO Haerter, and E Coppola. Statistical bias correction for daily precipitation in regional climate models over europe. *Theoretical and applied climatology*, 99:187–192, 2010.

[Qian and Chang, 2021] Weijia Qian and Howard H Chang. Projecting health impacts of future temperature: a comparison of quantile-mapping bias-correction methods. *International journal of environmental research and public health*, 18(4):1992, 2021.

[Qin *et al.*, 2021] Zequn Qin, Pengyi Zhang, Fei Wu, and Xi Li. Fcanet: Frequency channel attention networks. In *Proceedings of the IEEE/CVF international conference on computer vision*, pages 783–792, 2021.

[Ronneberger *et al.*, 2015] Olaf Ronneberger, Philipp Fischer, and Thomas Brox. U-net: Convolutional networks for biomedical image segmentation. In *Medical image computing and computer-assisted intervention–MICCAI 2015: 18th international conference, Munich, Germany, October 5-9, 2015, proceedings, part III 18*, pages 234–241. Springer, 2015.

[Shen *et al.*, 2021] Zhuoran Shen, Mingyuan Zhang, Haiyu Zhao, Shuai Yi, and Hongsheng Li. Efficient attention: Attention with linear complexities. In *Proceedings of the IEEE/CVF winter conference on applications of computer vision*, pages 3531–3539, 2021.

[Vaswani, 2017] A Vaswani. Attention is all you need. *Advances in Neural Information Processing Systems*, 2017.

[Venkataraman *et al.*, 2023] Shashanka Venkataraman, Amir Ghodrati, Yuki M Asano, Fatih Porikli, and Amirhossein Habibian. Skip-attention: Improving vision transformers by paying less attention. *arXiv preprint arXiv:2301.02240*, 2023.

[Wang *et al.*, 2018] Xiaolong Wang, Ross Girshick, Abhinav Gupta, and Kaiming He. Non-local neural networks. In *Proceedings of the IEEE conference on computer vision and pattern recognition*, pages 7794–7803, 2018.

[Wang *et al.*, 2020a] Haofan Wang, Zifan Wang, Mengnan Du, Fan Yang, Zijian Zhang, Sirui Ding, Piotr Mardziel, and Xia Hu. Score-cam: Score-weighted visual explanations for convolutional neural networks. In *Proceedings of the IEEE/CVF conference on computer vision and pattern recognition workshops*, pages 24–25, 2020.

[Wang *et al.*, 2020b] Qilong Wang, Banggu Wu, Pengfei Zhu, Peihua Li, Wangmeng Zuo, and Qinghua Hu. Eca-net: Efficient channel attention for deep convolutional neural networks. In *Proceedings of the IEEE/CVF conference on computer vision and pattern recognition*, pages 11534–11542, 2020.

[Wang *et al.*, 2024a] Hongjie Wang, Bhishma Dedhia, and Niraj K Jha. Zero-tprune: Zero-shot token pruning through leveraging of the attention graph in pre-trained transformers. In *Proceedings of the IEEE/CVF Conference on Computer Vision and Pattern Recognition*, pages 16070–16079, 2024.

[Wang *et al.*, 2024b] Kaishen Wang, Xun Xia, Jian Liu, Zhang Yi, and Tao He. Strengthening layer interaction via dynamic layer attention. *arXiv preprint arXiv:2406.13392*, 2024.

[Wang *et al.*, 2024c] Yan Wang, Yusen Li, Gang Wang, and Xiaoguang Liu. Multi-scale attention network for single image super-resolution. In *Proceedings of the IEEE/CVF Conference on Computer Vision and Pattern Recognition*, pages 5950–5960, 2024.

[Woo *et al.*, 2018] Sanghyun Woo, Jongchan Park, Joon-Young Lee, and In So Kweon. Cbam: Convolutional block attention module. In *Proceedings of the European conference on computer vision (ECCV)*, pages 3–19, 2018.

[Zhang *et al.*, 2023] Jing Zhang, Qiuge Qin, Qi Ye, and Tong Ruan. St-unet: Swin transformer boosted u-net with cross-layer feature enhancement for medical image segmentation. *Computers in Biology and Medicine*, 153:106516, 2023.

[Zhao *et al.*, 2021] Jingyu Zhao, Yanwen Fang, and Guodong Li. Recurrence along depth: Deep convolutional neural networks with recurrent layer aggregation. *Advances in Neural Information Processing Systems*, 34:10627–10640, 2021.

[Zhao *et al.*, 2022] Yue Zhao, Junzhou Chen, Zirui Zhang, and Ronghui Zhang. Ba-net: Bridge attention for deep convolutional neural networks. In *European Conference on Computer Vision*, pages 297–312. Springer, 2022.

Appendices

A Quantile Mapping

Algorithm 2 Quantile Mapping Algorithm

Input: A numerical set $\mathbf{X} = \{x_1, x_2, \dots, x_n\}$
Parameter: Target distribution F_θ with parameter θ
Output: Transformed set \mathbf{X}'

1: Compute the empirical cumulative probability for each x_i :

$$p(x_i) = \frac{1}{n} \sum_{j=1}^n \mathbb{I}(x_j \leq x_i), \quad p(x_i) \in [0, 1],$$

where $\mathbb{I}(\cdot)$ is the indicator function.

2: **for** $x_i \in \mathbf{X}$ **do**

3: Apply quantile mapping:

$$x'_i = F_\theta^{-1}(p(x_i)),$$

where F_θ^{-1} is the inverse CDF of the target distribution F_θ .

4: **end for**

5: **return** $\mathbf{X}' = \{x'_1, x'_2, \dots, x'_n\}$

Algorithm 2 outlines the original Quantile Mapping Algorithm as introduced by [Qian and Chang, 2021]. In this method, the Gamma distribution and Exponential distribution are frequently utilized to model the target distribution F_θ . Their cumulative distribution functions (CDFs) are as follows:

The CDF of the Gamma distribution is given by:

$$F_{\text{Gamma}}(x; \alpha, \beta) = \int_0^x \frac{t^{\alpha-1} e^{-t/\beta}}{\Gamma(\alpha) \beta^\alpha} dt$$

where α is the shape parameter, β is the scale parameter, and $\Gamma(\alpha)$ is the Gamma function, which is defined as:

$$\Gamma(\alpha) = \int_0^\infty t^{\alpha-1} e^{-t} dt$$

The CDF of the Exponential distribution is given by:

$$F_{\text{Exp}}(x; \lambda) = 1 - e^{-\lambda x}$$

where λ is the rate parameter of the distribution.

To assess the performance of EBQM in comparison to the existing Quantile Mapping Algorithms, we compared EBQM with the widely used Gamma Quantile Mapping (GQM) [Pianini *et al.*, 2010] and Exponential Quantile Mapping (EQM) methods [Heo *et al.*, 2019].

EBQM surpasses both GQM and EQM in Top-1 accuracy, achieving 74.31% and 75.35% for ResNet-56 and ResNet-110, respectively, as demonstrated in Table 7. These results surpass those of GQM, with accuracies of 74.02% and 74.98%, and EQM, with accuracies of 73.93% and 75.05%. Moreover, EBQM demonstrates the lowest standard deviation, at 0.24% and 0.22%, indicating superior stability when compared to GQM and EQM.

Depth	Algorithms	Top-1
56	GQM	74.02 \pm 0.38
	EQM	73.93 \pm 0.34
	EBQM	74.31\pm0.24
110	GQM	74.98 \pm 0.41
	EQM	75.05 \pm 0.37
	EBQM	75.35\pm0.22

Table 7: Top-1 accuracy (%) of different quantile mapping algorithms with ResNet backbone on CIFAR-100.

B Visualization

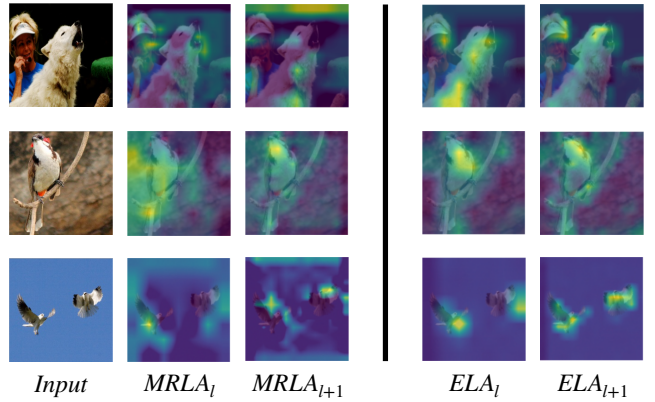


Figure 5

Figure 5 illustrates a comparison of the feature maps before and after the removal of redundant attention layers. The l -th and $l+1$ -th layers represent the attention layers identified for removal. It can be observed that by removing the MRLA layer while preserving the original ResNet backbone structure, the features extracted by these layers exhibit significant differences. Furthermore, it is evident that in certain layers, the removal of attention leads to the extraction of more precise features, thereby enhancing the model's representational capacity.

Figures 6 and 7 show the attention maps of MRLA on the CIFAR-100 dataset with ResNet-56 and the ImageNet-1K dataset with ResNet-50, respectively.

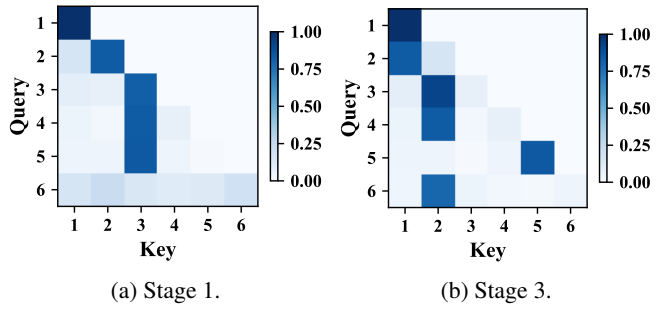
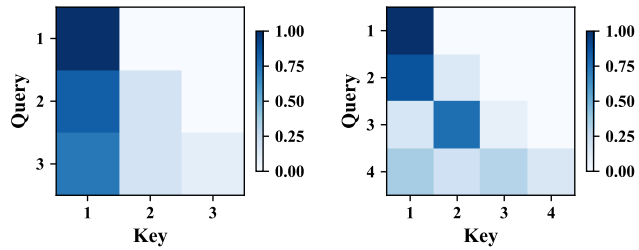
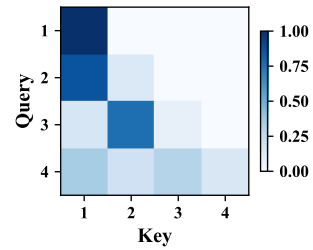


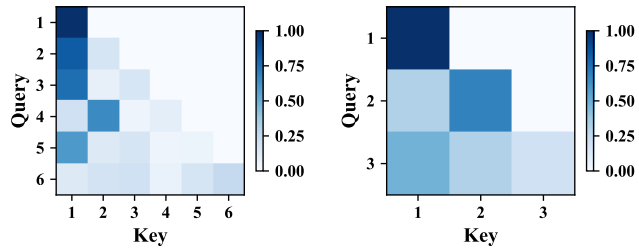
Figure 6: Visualization of attention scores at different stages of layer attention on the ResNet-56 backbone for CIFAR-100.



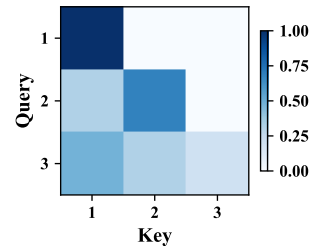
(a) Stage 1.



(b) Stage 2.



(c) Stage 3.



(d) Stage 4.

Figure 7: Visualization of attention scores at different stages of layer attention on the ResNet-50 backbone for ImageNet-1K.